J. Electrochem. Sci. Eng. **9(4)** (2019) 243-253; http://dx.doi.org/10.5599/jese.690

Open Access: ISSN 1847-9286
www.jESE-online.org

Original scientific paper

Sol-gel synthesis and electrochemical performance of $NiCo_2O_4$ nanoparticles for supercapacitor applications

Yong Zhang[1,2,✉], Yi Ru[1], Hai-Li Gao[1,✉], Shi-Wen Wang[1], Ji Yan[1], Ke-Zheng Gao[1], Xiao-Dong Jia[1], He-Wei Luo[1], Hua Fang[1], Ai-Qin Zhang[1] and Li-Zhen Wang[1]

[1]*Department of Material and Chemical Engineering, Zhengzhou University of Light Industry, Zhengzhou 450002, P.R. China*
[2]*Henan Provincial Key Laboratory of Surface & Interface Science, Zhengzhou University of Light Industry, Zhengzhou 450002, P.R. China*

Corresponding authors: ✉zy@zzuli.edu.cn; ✉gaohaili@zzuli.edu.cn

Received: April 4, 2019; Revised: June 7, 2019; Accepted: June 8, 2019

Abstract

In this work, $NiCo_2O_4$ nanoparticles with enhanced supercapacitive performance have been successfully synthesized via a facile sol-gel method and subsequent calcination in air. The morphology and composition of as-prepared samples were characterized using scanning electron microscopy (SEM), transmission electron microscope (TEM), X-ray diffraction (XRD), and Raman spectroscopy (Raman). The electrochemical performances of $NiCo_2O_4$ nanoparticles as supercapacitor electrode materials were evaluated by cyclic voltammetry (CV), galvanostatic charge/discharge (GCD) tests in 3 mol L^{-1} KOH aqueous solution. The results show that as-prepared $NiCo_2O_4$ nanoparticles have diameters of about 20-30 nm with uniform distribution. There are some interspaces between nanoparticles observed, which could increase the effective contact area with the electrolyte and provide fast path for the insertion and extraction of electrolyte ions. The electrochemical tests show that the prepared $NiCo_2O_4$ nanoparticles for supercapacitors exhibit excellent electrochemical performance with high specific capacitance and good cycle stability. The specific capacitance of $NiCo_2O_4$ electrode has been found as high as 1080, 800, 651, and 574 F g^{-1} at current densities of 1, 4, 7, and 10 A g^{-1}, respectively. Notably, the capacitance retention rate (compared with 1 A g^{-1}) is up to 74.1 %, 60.3 %, and 53.1 % at current densities of 4, 7, and 10 A g^{-1}, respectively. After 100 cycles, higher capacitance retention rate is also achieved. Therefore, the results indicate that $NiCo_2O_4$ material is the potential electrode material for supercapacitors.

Keywords

Supercapacitors, sol-gel method, $NiCo_2O_4$, nanoparticles, electrochemical performances

Introduction

Due to the rapid growth of global economy, depletion of fossil fuels and increasing environmental pollution, the search for "green" and renewable energy resources is one of the most urgent challenges facing us today. As one of the most promising energy storage devices, supercapacitors, also known as electrochemical capacitors or capacitors, are widely used in emergency power systems, hybrid electric vehicles, consumer electronics, industrial power systems, smart grids, aerospace, *etc*. This is due to their superior performances, such as high power density, nearly infinite cycle life, wide temperature range and high coulomb efficiency [1]. According to different storage mechanisms, supercapacitors are divided into two types [2]: electric double-layer capacitors (EDLCs) based on charge storage mechanisms at the electrode/electrolyte interface, and pseudocapacitors based on additional reversible redox reaction(s) of electrode materials. The electroactive materials of EDLCs are usually carbon-based materials [3] (such as activated carbon (AC), carbon nanotubes, carbon aerogels (CA), graphene, *etc.*), while the electrode materials of pseudocapacitors are mainly transition metal oxides and conductive polymers (such as RuO_2 [4], NiO [5], Co_3O_4 [6], MnO_2 [7], CeO_x [8], $NiCo_2O_4$ [9], Pr_6O_{11}@Ni-Co [10], $NiMoO_4$ [11], polyaniline [12], polypyrrole [13], *etc*.).

Pseudocapacitors can provide much higher specific capacitance than EDLCs by using reversible Faraday reactions on the electrode surface. Supercapacitor devices are composed of four parts: electrode materials (positive and negative), electrolyte, separator and shell, among which electrode materials play the key role in their performance. Unfortunately, the defects of electrode materials, such as low specific capacitance of carbon-based materials, poor electrochemical stability of conductive polymers, and poor electronic conductivity of transition metal oxides, seriously impede practical applications of supercapacitors [14]. Among pseudocapacitive materials, RuO_2, having specific capacity as high as 1580 F g^{-1} [15], is the most prominent electrode material for application in supercapacitors. However, the high cost and environmental toxicity hinder its extensive commercial application. Therefore, great efforts have been devoted to search cheap alternative materials with good capacitive characteristics similar to RuO_2, and especially those electrode materials with multiple oxidation states and high electronic conductivity.

In recent years, binary metal oxide/hydroxides have shown much better electronic conductivity and higher electrochemical activity than single component oxides/hydroxides [16], making them one of the most promising electrode materials for supercapacitors. As one of the binary metal oxides, $NiCo_2O_4$ is generally considered as a mixed valence oxide with pure spinel structure, in which nickel occupies octahedral sites and cobalt distributes in octahedral and tetrahedral sites [17]. The solid phase redox couples of Ni^{2+}/Ni^{3+} and Co^{2+}/Co^{3+} in this structure, present better electrocatalytic activity than single NiO and Co_3O_4, the conductivity that is at least twice higher than for NiO and Co_3O_4, and capacitive performance comparable with the noble metal oxide RuO_2. Therefore, $NiCo_2O_4$ has attracted considerable attention in energy conversion/storage systems due to its excellent electrochemical properties, rich redox reactions involving different ions, complex chemical components and synergistic effects. Hence, $NiCo_2O_4$ with ultra-high specific capacitance could be an alternative pseudocapacitive material to RuO_2. Currently, the spinel $NiCo_2O_4$ has been widely used in supercapacitors and lithium ion batteries, as electrocatalysts and magnetic materials, in photodetectors, ferrofluid technology, *etc.*[14,18].

Based on the pseudocapacitor mechanism, a golden way to improve the redox kinetics is to create nanostructured electrode materials with large surface area for redox reaction and short transport paths for ions and electrons. Therefore, the development of polymetallic oxide supercapacitor materials with special micro-nano structure and morphology is of great practical

significance and challenge. Thus far, various $NiCo_2O_4$ materials with different morphologies and nanostructures, such as nanowires [19], nanorods [20], urchin-like hollow microspheres [21], nanotubes [22], nanoneedles [23], nanosheets [24], *etc*., have been synthesized by various methods, including the sol-gel method [25], coprecipitation method [26], electrodeposition method [27], microwave method [28], and hydrothermal method [29]. In recent years, the ultracapacitors of $NiCo_2O_4$ have been studied [17,30]. However, due to the high calcination temperature, high crystallinity and low electrochemical activity, the specific capacitance of $NiCo_2O_4$ is low. Therefore, the development of pure $NiCo_2O_4$ by sol-gel technology is considered as a simple, cheap and low energy consumption method for the preparation of mixed metal oxides, which can produce homogeneous multi-component metal oxide materials with high purity, small grain size, large specific surface area, and good electrical conductivity.

In this work, we demonstrate use of a simple sol-gel method followed by calcination at moderate temperature of 350 °C, to prepare $NiCo_2O_4$ nanoparticles with unique characteristics. Some techniques such as scanning electron microscopy (SEM), X-ray diffraction (XRD), Raman spectroscopy (Raman), cyclic voltammetry (CV), and galvanostatic charge/discharge (GCD) methods were used to characterize the samples. The results show that the as-synthesized $NiCo_2O_4$ nanoparticles exhibit high specific capacitance, superior high-rate capability and long-life cycling stability. This is due to its small particle size, low crystallinity and high active materials utilization. Moreover, $NiCo_2O_4$ material benefits from multiple oxidation states/structures which contribute by both nickel and cobalt ions. These results indicate that the as-prepared $NiCo_2O_4$ nanoparticles have the potential application in development of high performance supercapacitors.

Experimental

Synthesis of $NiCo_2O_4$ nanoparticles

All reagents were of analytical level and used without further purification. Figure 1 presents the schematic diagram of the fabrication process of $NiCo_2O_4$ nanoparticles.

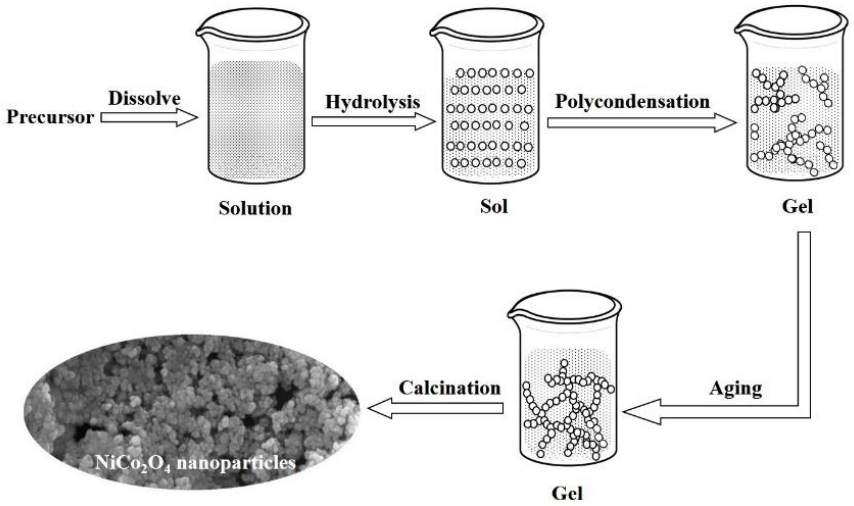

Figure 1. *Schematic diagram of $NiCo_2O_4$ nanoparticles preparation*

Firstly, 0.77 mmol of $Ni(NO_3)_2{\cdot}6H_2O$ and 1.54 mmol of $CoCl_2{\cdot}6H_2O$ were dissolved in 2.5 mL ethanol by ultrasonic treatment for 5 min, and then 0.025 g hexadecyl trimethyl ammonium bromide (CTAB) and 2.0 g propylene oxide were added to the dispersion and followed by stirring for 8 h at 25 °C. After reaction, the gel product was collected and cleaned by deionised water and

ethanol and dried at 60 °C for 12 h. Finally, the light green powder of the precursor was calcined in air atmosphere at 350 °C for 3 h in a muffle furnace to obtain the final $NiCo_2O_4$ nanoparticles.

Structure characterization

The morphologies and structures of the as-prepared $NiCo_2O_4$ nanoparticles were characterized by field emission scanning electron microscopy (SEM, JEOL JEM-7001F, Japan), transmission electron microscope (TEM, JEOL, JEM-700, Japan) and X-ray diffraction (XRD, D8 ADVANCE, Bruker Corporation). The composition and microstructure of the samples was performed on a Raman spectrometer (Raman, HORIBA, LABRAM HR800).

Electrode preparation and electrochemical measurements

The circular nickel foam with a diameter of 14 mm used as the working electrode current collector was firstly ultrasonicated for 10 min in 1 mol L^{-1} HCl solution, and then rinsed twice with acetone, ethanol and deionized water, respectively. Then, the cleaned nickel foam was put into a vacuum drying oven and dried at 60 °C for 12 h. The working electrode was prepared as follows. Firstly, the active material sample, carbon black and polyvinylidene fluoride (PVDF) were mixed with a mass ratio of 75:15:10 in an appropriate amount of N-methyl-2-pyrrolidone (NMP). The obtained mixture was ground to form the slurry, which was evenly coated on the surface of the treated nickel foam and dried at 60 °C for 8 h. The three-electrode system was used to determine the electrochemical performance of the working electrode. A platinum slice (2 × 2 cm) and Hg/HgO electrode were used as the counter and reference electrode, respectively. All measurements were performed in 3 mol L^{-1} KOH aqueous solution. The sample electrode was tested by using CHI 660E electrochemical workstation (Shanghai ChenhuaInstrument co., LTD.) in a three-port H-type cell for cyclic voltammetry (CV) and constant current charge-discharge (GCD) test. The scanning rates of CV tests were 2, 5, 10, 15 and 20 mV s^{-1} performed in the voltage scope of 0-0.5 V. GCD experiments were carried out in the potential range of 0-0.5 V with current densities of 1, 4, 7 and 10 A g^{-1}, respectively. The specific capacitance (C_m, F g^{-1}) values were calculated from charge-discharge curves according to the following equation (1):

$$C_m = \frac{C}{m} = \frac{i\Delta t}{m\Delta u} \quad (1)$$

In Eq. (1), i(A), m (g), $\triangle t$ (s) and $\triangle u$ (V) represent discharge current, mass of active electrode material, total discharge time and potential window, respectively.

Results and discussion

Structural characterization

The surface morphologies of $NiCo_2O_4$ samples were investigated by SEM with different magnifications. As shown in Figure 2, the sample is composed of many regular and disordered nanoparticles with a diameter of about 20-30 nm. Obviously, there are some loosely packed porous structures between the nanoparticles, with the size ranging from tens to hundreds of nanometers. This porous structure and interaction space between $NiCo_2O_4$ nanoparticles is beneficial for improving the specific surface area by enhancing the transport facility of ions, shortening the pathway of electron migration, maintaining the chemical stability during redox reactions, and improving the electrochemical performance. Therefore, as obtained $NiCo_2O_4$ nanomaterial is a promising candidate electrode material for supercapacitors.

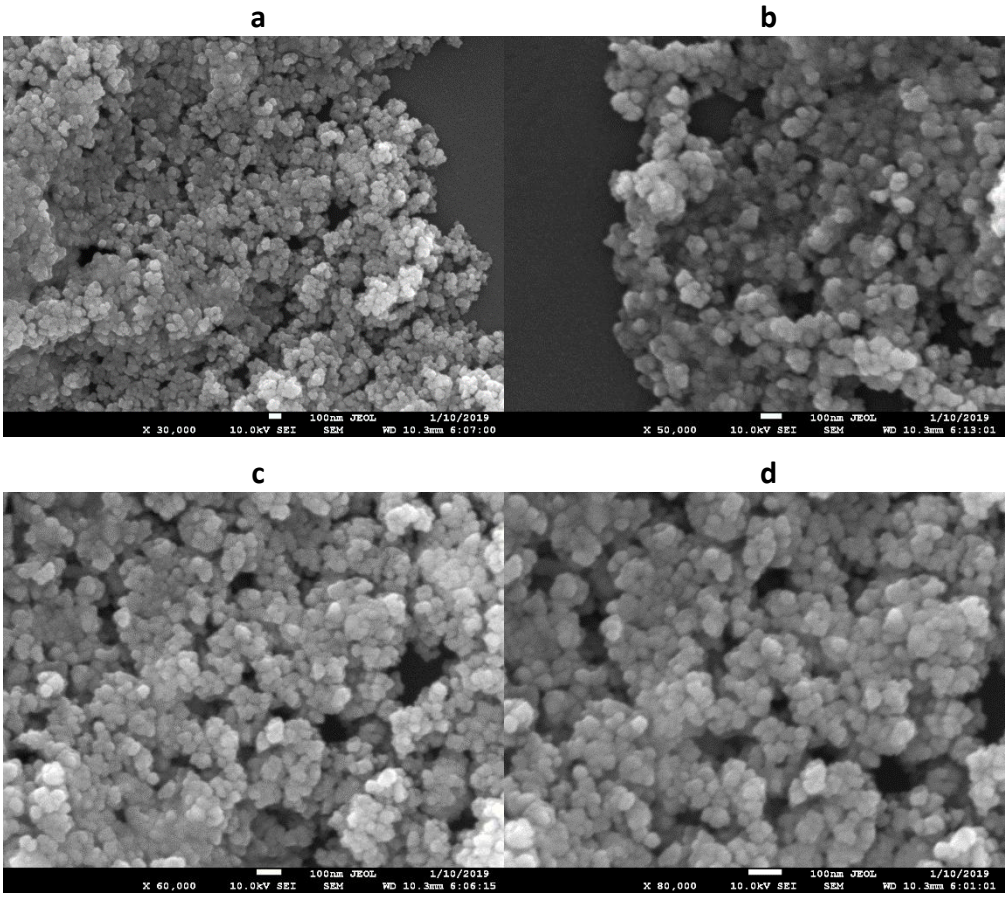

Figure 2. *SEM images of as-obtained $NiCo_2O_4$ nanoparticles at different magnifications: a- ×30000; b - ×50000; c - ×60000; d - ×80000.*

The detailed morphology, size and microstructure of the obtained $NiCo_2O_4$ nanoparticles were further examined by TEM. As shown in Figure 3(a) and (b), numerous nanoparticles are loosely packed together. In addition, Figure 3(c) and (d) show TEM magnification images of an individual diamond-like $NiCo_2O_4$ nanoparticles with a size of about 20-30 nm, in which the diamond-like structure contains a large number of nanopores. This unique porous structure will increase the contact area between the electrode and the electrolyte, which in turn will improve the electron and ion transport, improving thus electrochemical performance of the electrode [31].

The purity and crystal structure of the nickel foam substrate and as-prepared $NiCo_2O_4$ sample were determined by X-ray diffraction, and the corresponding XRD patterns are shown in Figure 4. It is found that all peaks located at 2 θ = 44.51, 51.85 and 76.37 ° can be perfectly indexed to (111), (200) and (220) planes of the nickel foam substrate (JCPDS 04-0850), respectively. The major diffraction peaks at 2θ = 31.15, 36.70, 44.62, 59.09 and 64.98° of $NiCo_2O_4$ (JCPDS No. 20-0781) correspond to the (220), (311), (400), (511) and (440) crystal planes, respectively [32]. It can be observed that all peaks in the pattern corroborate well with the standard pattern of face-centered cubic spinel $NiCo_2O_4$ with a space group of Fd3m. No excrescent peaks are detectable, indicating that the pure $NiCo_2O_4$ phase was successfully obtained. Moreover, broad and weak diffraction peaks indicate that $NiCo_2O_4$ exhibited inferior crystallinity and nanocrystallinity, which are favorable for $NiCo_2O_4$ nanoparticles to exhibit better capacitive performance [25].

To further evaluate the phase formation and structural features of the prepared $NiCo_2O_4$ nanoparticles, Raman spectroscopy was performed with a typical spectral range of 150-750 cm^{-1}, and the typical Raman spectrum of the sample is shown in Figure 5.

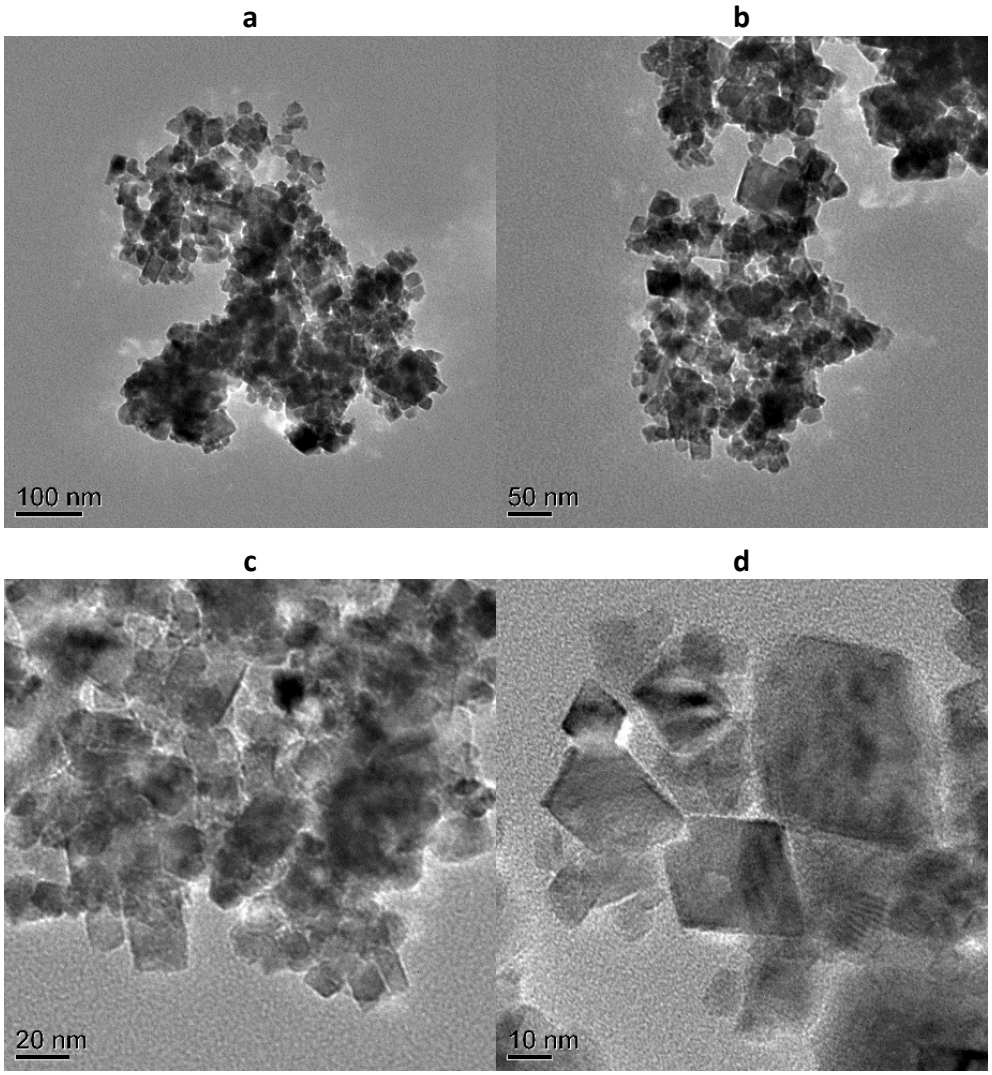

Figure 3. *TEM images of as-obtained $NiCo_2O_4$ nanoparticles at different magnifications*

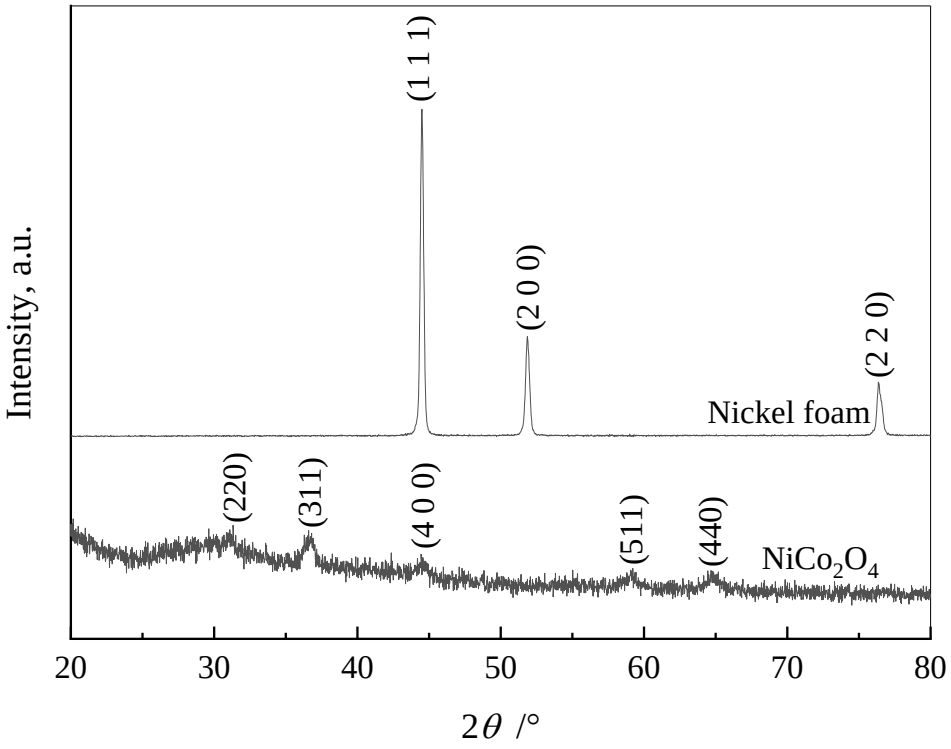

Figure 4. *XRD patterns of the nickel foam substrate and as-prepared $NiCo_2O_4$ nanoparticles*

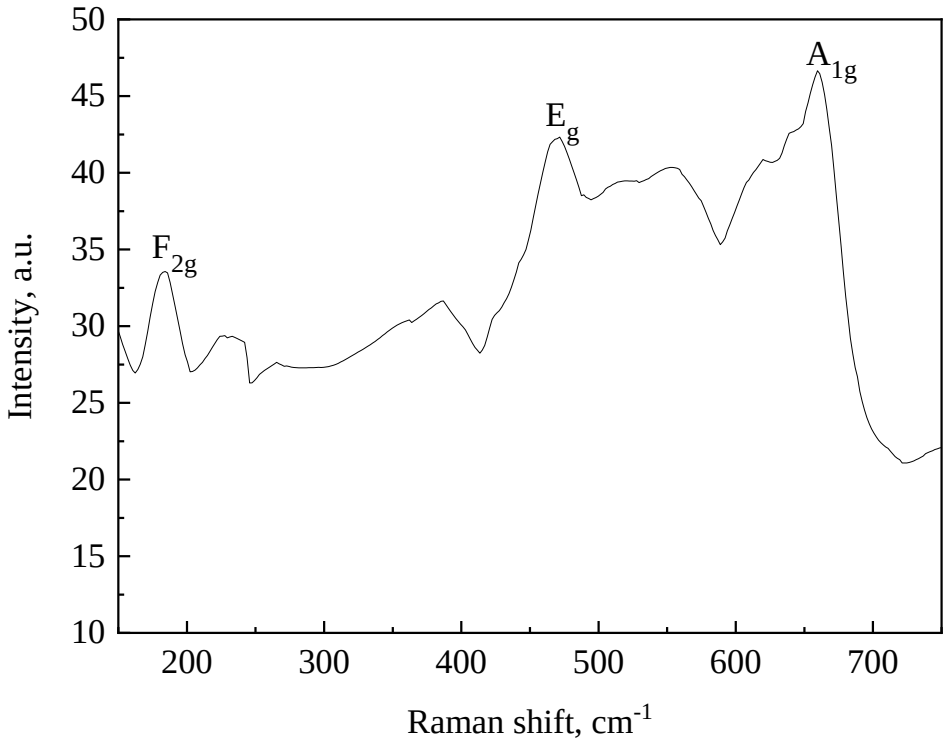

Figure 5. *Raman spectrum of the as-prepared $NiCo_2O_4$ nanoparticles*

The stretching vibration peaks observed at ~182.2 , ~469.1, and ~661.1 cm^{-1} correspond to F_{2g}, E_g and A_{1g} modes of $NiCo_2O_4$ respectively, confirming its single-phase formation of spinel structure. The observed mode of the phonon is attributed to the vibration of Co-O and Ni-O, respectively [33]. Moreover, $NiCo_2O_4$ samples show only Co-O and Ni-O vibrations, indicating that the precursors of nickel and cobalt were completely decomposed at 350 °C, what is consistent with the literature [34] and implies that pure $NiCo_2O_4$ was formed after calcination. These results are well consistent with the XRD results, which further confirm the formation of $NiCo_2O_4$ nanoparticles.

Electrochemical characterization

The electrochemical capacitive performance of the as-prepared $NiCo_2O_4$ sample was evaluated by CV measurements using a three-electrode system. Figure 6 shows CVs recorded for $NiCo_2O_4$ nanoparticles in 3 mol L^{-1} KOH aqueous electrolyte. The potential was scanned between 0 and 0.5 V at scanning rates of 2, 5, 10, 15 and 20 mVs^{-1}, respectively. A pair of redox peaks can be detected in each voltammogram, indicating that the electrode capacitance is mainly based on the redox mechanism related to reversible redox reactions of Ni^{2+}/Ni^{3+} and Co^{3+}/Co^{4+}, associated with anions OH^- [35]. As can be seen from CV curves in Figure 6, the anodic peak potential at around ~0.48 V and cathodic peak potential at ~0.36 V are noticed at the scan rate of 2 mVs^{-1}, which is close to the literature value. Moreover, when the scanning rate increased from 5 to 20 mVs^{-1}, the position of the anodic peak shifts slightly from 0.48 to 0.50 V, indicating that the electrode material resistance is relatively low and electrochemical reversibility is good [18].

To further estimate the supercapacitive performance of the as-prepared $NiCo_2O_4$ nanoparticles, GCD measurements were carried out within the potential range from 0 to 0.5 V at current densities of 1, 4, 7 and 10 A g^{-1}, respectively. As shown in Figure 7, the charge-discharge curves are non-linear with an obvious plateau at around 0.45 V and 0.39 V. This is well consistent with CV results and further verifies the pseudocapacitive behavior and good reversibility of the redox process at $NiCo_2O_4$ electrode [18].

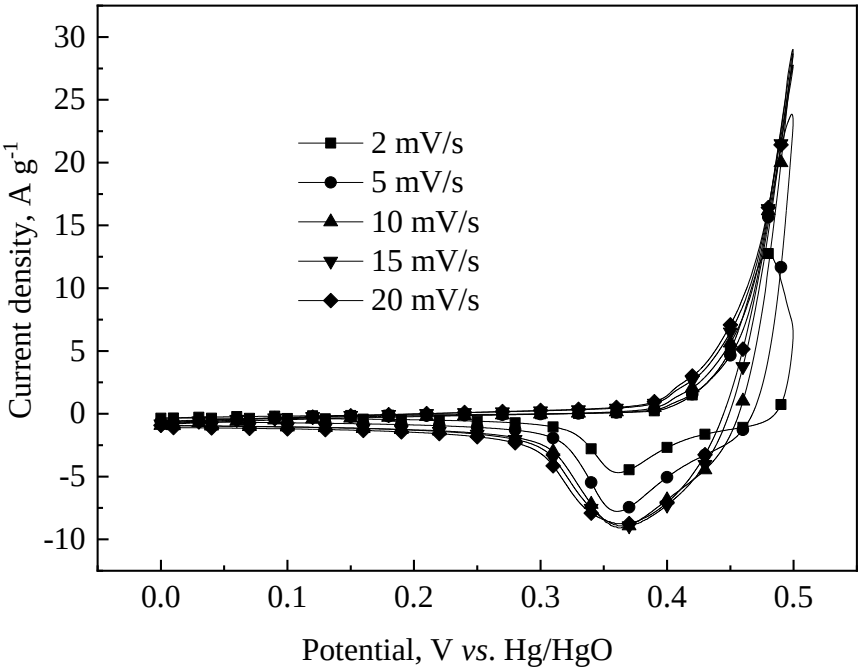

Figure 6. *CV curves of as-prepared $NiCo_2O_4$ electrode in a three-electrode system scanned between 0 and 0.5 V at various scan rates*

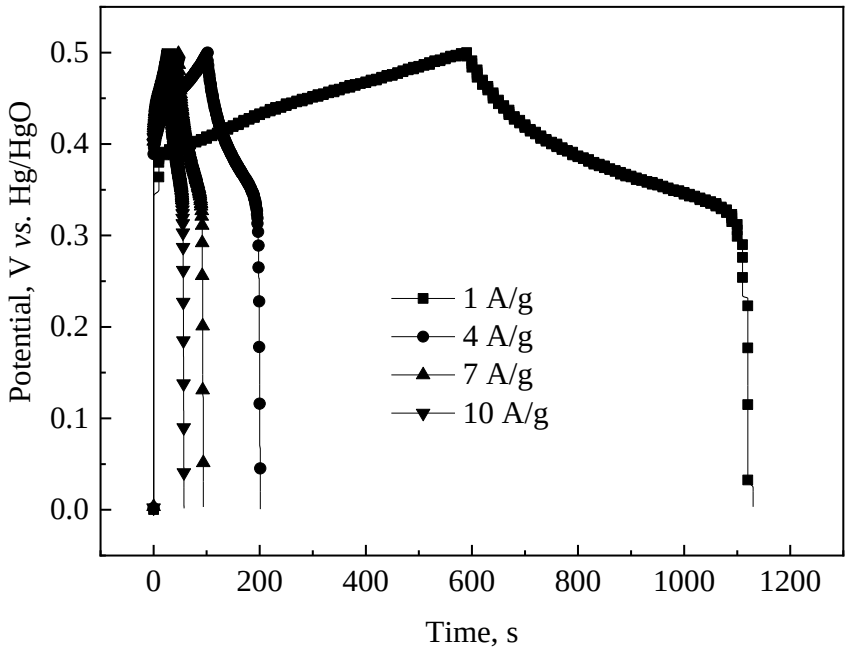

Figure 7. *GCD curves of as-prepared $NiCo_2O_4$ electrode at various current densities between 0 and 0.5 V*

Based on the discharge curves, the specific capacitances of the as-prepared $NiCo_2O_4$ electrode were calculated according to Eq. (1), and the results are illustrated in Figure 8. Specific capacitances of as-prepared $NiCo_2O_4$ are as high as 1080, 800, 651 and 574 F g^{-1} at discharge current densities of 1, 4, 7 and 10 A g^{-1}, respectively. Compared with the current density of 1 A g^{-1}, the retained capacitances were still 74.1, 60.3 and 53.1 %, even the current density was increased to 4, 7 and 10 A g^{-1}, what suggests good retention rate performance. The excellent electrochemical properties of $NiCo_2O_4$ nanoparticles can be attributed to the small particle size, which will increase the contact area of electrolyte/electrode, thus providing more active sites for rapid redox reactions which undoubtedly contributes to the high capacitance [35]. Besides, the nanoporous structure between the particles also allows the electrolyte ions to be transported quickly into the bulk materials, what further enhances the electrode rate capability.

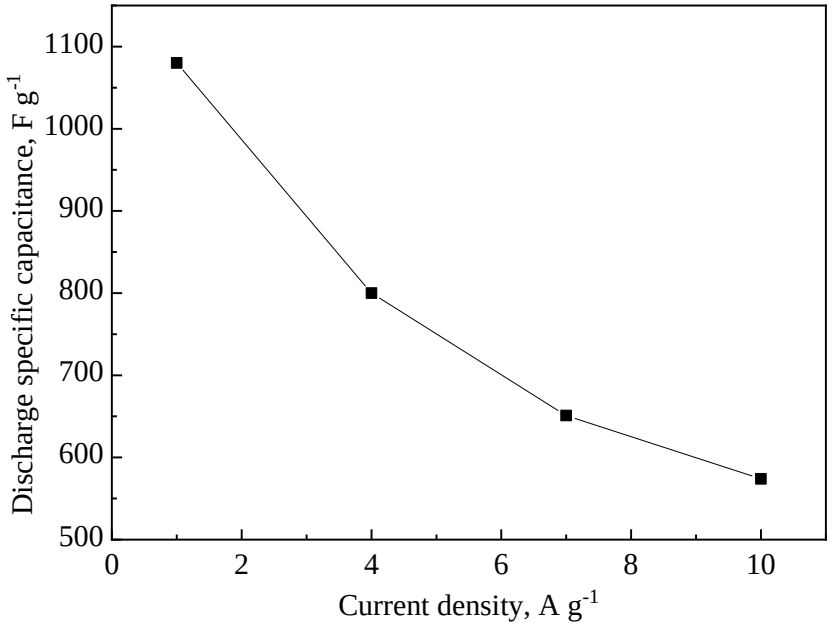

Figure 8. *Specific capacitance of as-prepared $NiCo_2O_4$ electrode as a function of discharge current density*

The cycling stability of the as-prepared $NiCo_2O_4$ electrode in 3 mol L^{-1} KOH aqueous electrolyte was examined by applying 100 cycles within the potential range of 0-0.5 V at current densities of 4, 7 and 10 A g^{-1}, and the results are shown in Figure 9. During the cycling, the specific capacitance of the as-prepared $NiCo_2O_4$ electrode remained almost unchanged at all current densities. The initial discharge specific capacitance of $NiCo_2O_4$ electrode is 800, 651 and 574 F g^{-1} at the current density of 4,7 and 10 A g^{-1}, respectively. After 100 cycles, the specific capacitance decreases to 758, 597 and 521 F g^{-1}, showing that the corresponding specific capacitance retention rates were 94.8, 91.7 and 90.8 % and indicating that $NiCo_2O_4$ electrode has good electrochemical stability. Better cyclic stability can be attributed to the unique pore structure, which can be used as the "release zone" of ions and internal nanogrids that buffers possible volume changes due to OH^- ions insertion/extraction process during cycling, improving thus its structural stability.

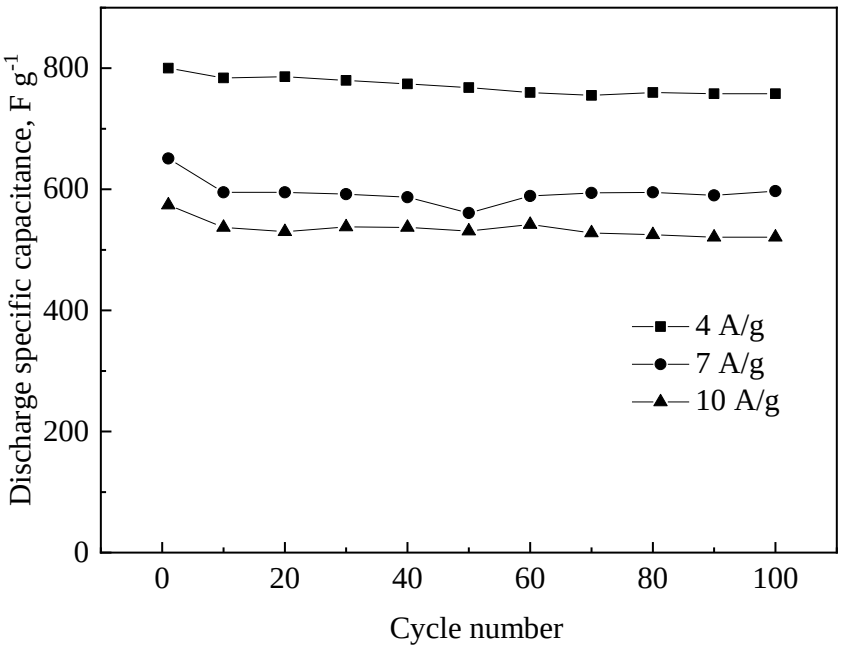

Figure 9. *Cyclic stability of as-prepared $NiCo_2O_4$ electrode at various discharge current densities*

Conclusion

By using $Ni(NO_3)_2{\cdot}6H_2O$ and $CoCl_2{\cdot}6H_2O$ as raw materials, a promising electrode material, $NiCo_2O_4$ nanoparticles, were synthesized successfully *via* the sol-gel process followed by calcining at 350 °C. In the unique structure of synthesized nanoparticles, there are obvious porous structures formed among large number of nanoparticles, which provide an effective way for rapid reversible reaction, improving thus electrochemical properties of $NiCo_2O_4$ material. Electrochemical characterization showed high specific capacitance, good rate capability and good cycling stability of the prepared $NiCo_2O_4$ nanomaterial. High specific capacitance of 1080 F g^{-1} was achieved at the current density of 1 A g^{-1}, while specific capacitances of 800, 651 and 574 F g^{-1}were obtained at the discharge current densities of 4, 7 and 10 A g^{-1}, respectively. After 100 cycles, the specific capacitance decreases to 758, 597 and 521 F g^{-1}, suggesting the corresponding specific capacitance retention rates of 94.8, 91.7 and 90.8 %. The excellent electrochemical capacitive performance, low cost, simple and easy fabrication of the as-prepared $NiCo_2O_4$ nanoparticles render this material as the promising electrochemical capacitor electrode material.

Acknowledgments: *This work is supported by the Program for Science & Technology Innovation Team in Universities of Henan Province (Grant No. 16IRTSTHN016), the National Natural Science Foundation of China (Grant No. 21503193), and the National Natural Science Foundation of China (Grant No. U1404201).*

References

[1] Y. Zhang, H. Feng, X. Wu, L. Wang, A. Zhang, T. Xia, H. Dong, X. Li and L. Zhang, *International Journal of Hydrogen Energy* **34** (2009) 4889-4899.
[2] Y. Li, X. Han, T. Yi, Y. He and X. Li, *Journal of Energy Chemistry* **31** (2019) 54-78.
[3] W. Gu and G. Yushin, *Wiley Interdisciplinary Reviews: Energy and Environment* **3** (2014) 424-473.
[4] J. Sun, E. Lei, C. Ma, Z. Wu, Z. Xu, Y. Liu, W. Li and S. Liu, *Electrochimica Acta* **300** (2019) 225-234.
[5] Y. Jiao, W. Hong, P. Li, L. Wang and G. Chen, *Applied Catalysis B: Environmental* **244** (2019) 732-739.
[6] Y. Duan, T. Hu, L. Yang, J. Gao, S. Guo, M. Hou and X. Ye, *Journal of Alloys and Compounds* **771** (2019) 156-161.
[7] Y. Zhang, Q.-q. Yao, H.-l. Gao, L.-s. Zhang, L.-z. Wang, A.-q. Zhang, Y.-h. Song and L.-x. Wang, *Journal of Analytical and Applied Pyrolysis* **111** (2015) 233-237.
[8] A. Younis, D. Chu and S. Li, *Journal of Materials Chemistry A* **3** (2015) 13970-13977.
[9] Y. Z. Ma, Z. X. Yu, M. M. Liu, C. Song, X. N. Huang, M. Moliere, G. S. Song and H. L. Liao, *Ceramics International* **45** (2019) 10722-10732.
[10] N. Chen, A. Younis, S. Huang, D. Chu and S. Li, *Journal of Alloys and Compounds* **783** (2019) 772-778.
[11] Y. Zhang, H.-l. Gao, X.-d. Jia, S.-w. Wang, J. Yan, H.-w. Luo, K.-z. Gao, H. Fang, A.-q. Zhang and L.-z. Wang, *Journal of Renewable and Sustainable Energy* **10** (2018) 054101-054110.
[12] H. Zhou, X. Zhi, W. Zhang and H.-J. Zhai, *Organic Electronics* **69** (2019) 98-105.
[13] Q. Zhang, B. Sun, J. Sun, N. Wang and W. Hu, *Journal of Electroanalytical Chemistry* **839** (2019) 39-47.
[14] L. Liu, H. Zhang, L. Fang, Y. Mu and Y. Wang, *Journal of Power Sources* **327** (2016) 135-144.
[15] X. Y. Liu, Y. Q. Zhang, X. H. Xia, S. J. Shi, Y. Lu, X. L. Wang, C. D. Gu and J. P. Tu, *Journal of Power Sources* **239** (2013) 157-163.
[16] Z. Z. Zeng, L. Z. Zhu, E. S. Han, X. C. Xiao, Y. R. Yao and L. M. Sun, *Ionics* **25** (2019) 2791-2803.
[17] Y. Q. Wu, X. Y. Chen, P. T. Ji and Q. Q. Zhou, *Electrochimica Acta* **56** (2011) 7517-7522.
[18] Y. Zhu, X. Pu, W. Song, Z. Wu, Z. Zhou, X. He, F. Lu, M. Jing, B. Tang and X. Ji, *Journal of Alloys and Compounds* **617** (2014) 988-993.
[19] S. Li, K. Yang, P. Ye, H. Jiang, Z. Zhang, Q. Huang and L. Wang, *Applied Surface Science* **473** (2019) 326-333.
[20] W. Zhang, W. Xin, T. Hu, Q. Gong, T. Gao and G. Zhou, *Ceramics International* **45** (2019) 8406-8413.
[21] Y. Luo, R. Guo, T. Li, F. Li, L. Meng, Z. Yang, Y. Wan and H. Luo, *ChemElectroChem* **6** (2019) 690-699.
[22] H.-L. Fan, J. Zhang, W. Ju, B.-X. Liu, X.-F. Zhao, X.-C. Liu and X.-B. Yi, *International Journal of Nanomanufacturing* **15** (2019) 92-104.

[23] Y. L. D. LI, R. Chen, H NI, *Acta Metallurgica* **54** (2018) 1179-1186.
[24] J. Dai, R. Zhao, J. Xiang, F. Wu, L. Xin, Y. Zhang and S. Ma, *Science of Advanced Materials* **11** (2019) 379-385.
[25] M. C. Liu, L. B. Kong, C. Lu, X. M. Li, Y. C. Luo and L. Kang, *ASC Applied Materials & Interfaces* **4** (2012) 4631-4636.
[26] Z. Wu, Y. Zhu and X. Ji, *Journal of Materials Chemistry A* **2** (2014) 14759-14772.
[27] N. Wang, B. Sun, P. Zhao, M. Yao, W. Hu and S. Komarneni, *Chemical Engineering Journal* **345** (2018) 31-38.
[28] Y. Xiao, Y. Lei, B. Zheng, L. Gu, Y. Wang and D. Xiao, *RSC Advances* **5** (2015) 21604-21613.
[29] S. N. Gao, F. Liao, S. Z. Ma, L. L. Zhu and M. W. Shao, *Journal of Materials Chemistry A* **3** (2015) 16520-16527.
[30] H.-W. Wang, Z.-A. Hu, Y.-Q. Chang, Y.-L. Chen, H.-Y. Wu, Z.-Y. Zhang and Y.-Y. Yang, *Journal of Materials Chemistry* **21** (2011) 10504-10511.
[31] L. Ma, X. Shen, Z. Ji, X. Cai, G. Zhu and K. Chen, *Journal of Colloid and Interface Science* **440** (2015) 211-218.
[32] C. Wang, X. Zhang, D. Zhang, C. Yao and Y. Ma, *Electrochimica Acta* **63** (2012) 220-227.
[33] S. Karmakar, S. Varma and D. Behera, *Journal of Alloys and Compounds* **757** (2018) 49-59.
[34] P. Bhojane, S. Sen and P. M. Shirage, *Applied Surface Science* **377** (2016) 376-384.
[35] Y. Zhu, X. Ji, Z. Wu, W. Song, H. Hou, Z. Wu, X. He, Q. Chen and C. E. Banks, *Journal of Power Sources* **267** (2014) 888-900.